
Robust Optimal Transport with Applications in Generative Modeling and Domain Adaptation

Yogesh Balaji

Department of Computer Science
University of Maryland
College Park, MD
yogesh@umd.edu

Rama Chellappa

Electrical and Computer Engineering
and Biomedical Engineering Departments
Johns Hopkins University
Baltimore, MD
rchella4@jhu.edu

Soheil Feizi

Department of Computer Science
University of Maryland
College Park, MD
sfeizi@cs.umd.edu

Abstract

Optimal Transport (OT) distances such as Wasserstein have been used in several areas such as GANs and domain adaptation. OT, however, is very sensitive to outliers (samples with large noise) in the data since in its objective function, every sample, including outliers, is weighed similarly due to the marginal constraints. To remedy this issue, robust formulations of OT with unbalanced marginal constraints have previously been proposed. However, employing these methods in deep learning problems such as GANs and domain adaptation is challenging due to the instability of their dual optimization solvers. In this paper, we resolve these issues by deriving a computationally-efficient dual form of the robust OT optimization that is amenable to modern deep learning applications. We demonstrate the effectiveness of our formulation in two applications of GANs and domain adaptation. Our approach can train state-of-the-art GAN models on noisy datasets corrupted with outlier distributions. In particular, our optimization computes weights for training samples reflecting how difficult it is for those samples to be generated in the model. In domain adaptation, our robust OT formulation leads to improved accuracy compared to the standard adversarial adaptation methods. Our code is available at <https://github.com/yogeshbalaji/robustOT>.

1 Introduction

Estimating distances between probability distributions lies at the heart of several problems in machine learning and statistics. A class of distance measures that has gained immense popularity in several machine learning applications is Optimal Transport (OT) [29]. In OT, the distance between two probability distributions is computed as the minimum cost of transporting a source distribution to the target one under some transportation cost function. Optimal transport enjoys several nice properties including structure preservation, existence in smooth and non-smooth settings, being well defined for discrete and continuous distributions [29], etc.

Two recent applications of OT in machine learning include generative modeling and domain adaptation. In Wasserstein GAN [1], a generative model is trained by minimizing the (approximate) Wasserstein distance between real and generative distributions. In the dual form, this objective

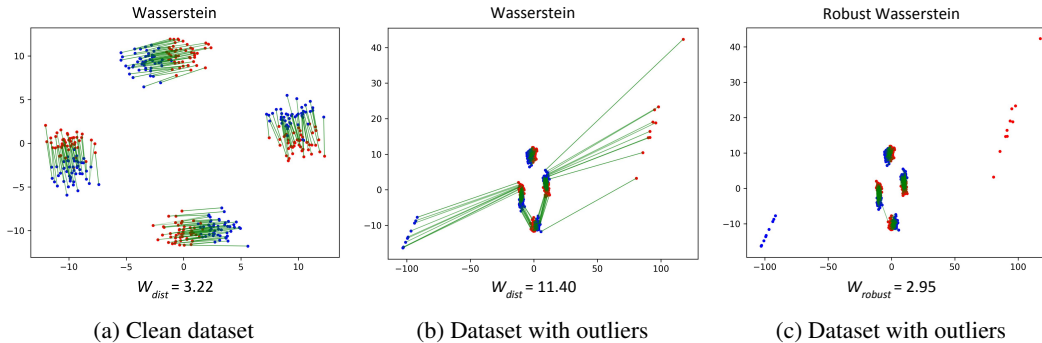


Figure 1: Visualizing couplings of Wasserstein computation between two distributions shown in red and blue. In (a), we show the couplings when no outliers are present. In (b), we show the couplings when 5% outliers are added to the data. The Wasserstein distance increases significantly indicating high sensitivity to outliers. In (c), we show the couplings produced by the Robust Wasserstein measure. Our formulation effectively ignores the outliers yielding a Wasserstein estimate that closely approximates the true Wasserstein distance.

reduces to a two-player *min-max* game between a generator and a discriminator. Similar ideas involving distance minimization between source and target feature distributions are common in domain adaptation [10]. In [26, 2], Wasserstein distance is used as the choice of distance measure for minimizing the domain gap.

One of the fundamental shortcomings of optimal transport is its sensitivity to outlier samples. By outliers, we mean samples with large noise. In the OT optimization, to satisfy the marginal constraints between the two input distributions, every sample is weighed equally in the feasible transportation plans. Hence, even a few outlier samples can contribute significantly to the OT objective. This leads to poor estimation of distributional distances when outliers are present. An example is shown in Fig. 1, where the distance between distributions shown in red and blue are computed. In the absence of outliers (Fig. 1(a)), proper couplings (shown in green) are obtained. However, even in the presence of a very small fraction of outliers (as small as 5%), poor couplings arise leading to a large change in the distance estimate (Fig. 1(b)).

The OT sensitivity to outliers is undesirable, especially when we deal with large-scale datasets where the noise is inevitable. This sensitivity is a consequence of exactly satisfying the marginal constraints in OT’s objective. Hence, to boost OT’s robustness against outliers, we propose to utilize recent formulations of unbalanced optimal transport [6, 13] which relax OT’s marginal constraints. The authors in [6, 13] provide an exact dual form for the unbalanced OT problem. However, we have found that using this dual optimization in large-scale deep learning applications such as GANs results in poor convergence and an unstable behaviour (see Section 3.1 and the appendix for details).

To remedy this issue, in this work, we derive a computationally efficient dual form for the unbalanced OT optimization that is suited for practical deep learning applications. Our dual simplifies to a weighted OT objective, with low weights assigned to outlier samples. These instance weights can also be useful in interpreting the difficulty of input samples for learning a given task. We develop two solvers for this dual problem based on either a discrete formulation or a continuous stochastic relaxation. These solvers demonstrate high stability in large-scale deep learning applications.

We show that, under mild assumptions, our robust OT measure (which is similar in form to the unbalanced OT) is upper bounded by a constant factor of the true OT distance (OT ignoring outliers) for any outlier distribution. Hence, our robust OT can be used for effectively handling outliers. This is visualized in Figure 1(c), where couplings obtained by robust OT effectively ignores outlier samples, yielding a good estimate of the true OT distance. We demonstrate the effectiveness of the proposed robust OT formulation in two large-scale deep learning applications of generative modeling and domain adaptation. In generative modeling, we show how robust Wasserstein GANs can be trained using state-of-the-art GAN architectures to effectively ignore outliers in the generative distribution. In domain adaptation, we utilize the robust OT framework for the challenging task of synthetic to real adaptation, where our approach improves adversarial adaptation techniques by $\sim 5\%$.

2 Background on Optimal Transport

Let \mathcal{X} denote a compact metric space, and $Prob(\mathcal{X})$ denote the space of probability measures defined on \mathcal{X} . Given two probability distributions $\mathbb{P}_X, \mathbb{P}_Y \in Prob(\mathcal{X})$ and a continuous cost function $c: \mathcal{X} \times \mathcal{X} \rightarrow \mathbb{R}$, optimal transport finds the minimum cost for transporting the density \mathbb{P}_X to \mathbb{P}_Y [29], given by the following cost function

$$\mathcal{W}(\mathbb{P}_X, \mathbb{P}_Y) = \min_{\pi \in \Pi(\mathbb{P}_X, \mathbb{P}_Y)} \int \int c(x, y) \pi(x, y) dx dy \quad (1)$$

where $\Pi(\mathbb{P}_X, \mathbb{P}_Y)$ is set of all joint distributions (couplings) whose marginals are \mathbb{P}_X and \mathbb{P}_Y , respectively. That is, $\int \pi(x, y) dy = \mathbb{P}_X$ and $\int \pi(x, y) dx = \mathbb{P}_Y$. These set of constraints enforce that the marginals of couplings exactly match the distributions \mathbb{P}_X and \mathbb{P}_Y . Hence, when the input distributions have outliers, they are forced to have non-zero weights in couplings leading to a large transportation cost. In practice, the dual form of the optimization (1) is often used.

Kantrovich Duality: The dual formulation of optimal transport problem [29] is given by:

$$\min_{\pi \in \Pi(\mathbb{P}_X, \mathbb{P}_Y)} \int \int c(x, y) \pi(x, y) dx dy = \max_{\phi \in Lip-1} \int \phi(x) d\mathbb{P}_X - \int \phi(x) d\mathbb{P}_Y. \quad (2)$$

Optimization (2) is the celebrated *Kantorovich-Rubinstein* duality. This is a simpler optimization problem compared to (1) since the maximization is over a class of 1-Lipschitz functions. In practice, $\phi(\cdot)$ function is implemented using a neural network, and the 1-Lipschitz constraint is enforced using weight clipping [1] or a penalty on the gradients [11].

The use of optimal transport has gained popularity in machine learning [28, 26, 1], computer vision [27, 4] and many other disciplines. Several relaxations of the OT problem have been proposed in the literature. Two popular ones include entropy regularization [8, 3] and marginal relaxation [13, 6, 7, 9, 12]. In this work, we utilize the marginal relaxations of [13, 6] for handling outlier noise in machine learning applications involving OT. To the best of our knowledge, ours is the first work to demonstrate the utility of unbalanced OT in large-scale deep learning applications. Only other paper that is similar in spirit to our work is [30]. However, [30] provides a relaxation for the Monge unbalanced OT, which is different from the unbalanced Kantrovich problem we consider in this paper.

3 Robust Optimal Transport

Our objective is to handle outliers in deep learning applications involving OT. For this, we use relaxed OT formulations. In this section, we first formally define the outlier model we use. Then, we discuss the existing marginal relaxation formulations in OT and the issues that arise in deep learning when using these formulations. We then propose a reformulation of the dual that is suited for deep learning.

Outlier Model: We consider outliers as samples with large noise. More specifically, let \mathbb{P}_X and \mathbb{P}_Y be two distributions whose Wasserstein distance we desire to compute. Let $\mathbb{P}_X = \alpha \mathbb{P}_X^c + (1 - \alpha) \mathbb{P}_X^a$; i.e., the clean distribution \mathbb{P}_X^c is corrupted with $(1 - \alpha)$ fraction of noise \mathbb{P}_X^a . Then, \mathbb{P}_X^a is considered an outlier distribution if $\mathcal{W}(\mathbb{P}_X^c, \mathbb{P}_Y) \ll \mathcal{W}(\mathbb{P}_X^a, \mathbb{P}_Y)$. For an example, refer to Fig. 1(b).

3.1 Unbalanced Optimal Transport

As seen in Fig. 1, sensitivity to outliers arises due to the marginal constraints in OT. If the marginal constraints are relaxed in a way that the transportation plan does not assign large weights to outliers, they can effectively be ignored. [6, 13] have proposed one such relaxation using f -divergence on marginal distributions. This formulation, called *Unbalanced Optimal Transport*, can be written as

$$\mathcal{W}^{ub}(\mathbb{P}_X, \mathbb{P}_Y) = \min_{\pi \in \Pi(\mathbb{P}_{\tilde{X}}, \mathbb{P}_{\tilde{Y}})} \int c(x, y) \pi(x, y) dx dy + \mathcal{D}_f(\mathbb{P}_{\tilde{X}} || \mathbb{P}_X) + \mathcal{D}_f(\mathbb{P}_{\tilde{Y}} || \mathbb{P}_Y) \quad (3)$$

where \mathcal{D}_f is the f -divergence between distributions, defined as $\mathcal{D}_f(P||Q) = \int f(\frac{dP}{dQ}) dQ$. Furthermore, [13] derived a dual form for the problem. Let f be a convex lower semi-continuous function.

Define $r^*(x) := \sup_{s>0} \frac{x-f(s)}{s}$ where $f'_\infty := \lim_{s \rightarrow \infty} \frac{f(s)}{s}$. Then,

$$\begin{aligned} \mathcal{W}^{ub}(\mathbb{P}_X, \mathbb{P}_Y) &= \max_{\phi, \psi} \int \phi(x) d\mathbb{P}_X + \int \psi(y) d\mathbb{P}_Y \\ \text{s.t. } &r^*(\phi(x)) + r^*(\psi(y)) \leq c(x, y) \end{aligned} \quad (4)$$

Computational issues using this dual form in deep learning: Training neural networks using this dual form is challenging as it involves maximizing over *two* discriminator functions (ϕ and ψ), with constraints connecting these functions. For χ^2 divergence, we derived the GAN objective using this dual and trained a model. However, we were unsuccessful in making the model converge using standard SGD as it showed severe instability. Please refer to Appendix for more details. This limits the utility of this formulation in deep learning applications. In what follows, we present a reformulation of the dual that is scalable and suited for deep learning applications.

3.2 Our Duality

We start with a slightly different form than (3) where we keep the f -divergence relaxations of marginal distributions as constraints:

$$\begin{aligned} \mathcal{W}_{\rho_1, \rho_2}^{rob}(\mathbb{P}_X, \mathbb{P}_Y) &:= \min_{\mathbb{P}_{\tilde{X}}, \mathbb{P}_{\tilde{Y}} \in Prob(\mathcal{X})} \min_{\pi \in \Pi(\mathbb{P}_{\tilde{X}}, \mathbb{P}_{\tilde{Y}})} \int \int c(x, y) \pi(x, y) dx dy \\ \text{s.t. } &\mathcal{D}_f(\mathbb{P}_{\tilde{X}} || \mathbb{P}_X) \leq \rho_1, \mathcal{D}_f(\mathbb{P}_{\tilde{Y}} || \mathbb{P}_Y) \leq \rho_2. \end{aligned} \quad (5)$$

In this formulation, we optimize over the couplings whose marginal constraints are the relaxed distributions $\mathbb{P}_{\tilde{X}}$ and $\mathbb{P}_{\tilde{Y}}$. To prevent over-relaxation of the marginals, we impose a constraint that the f -divergence between the relaxed and the true marginals are bounded by constants ρ_1 and ρ_2 for distributions $\mathbb{P}_{\tilde{X}}$ and $\mathbb{P}_{\tilde{Y}}$, respectively. As seen in Fig. 1(c), this relaxation effectively ignores the outlier distributions when (ρ_1, ρ_2) are chosen appropriately. We study some properties of robust OT in the appendix. Notably, robust OT does not satisfy the triangle inequality.

Note that the Lagrangian relaxation of optimization (5) takes a similar form to that of the unbalanced OT objective (3). Having a hard constraint on f -divergence gives us an explicit control over the extent of the marginal relaxation which is suited for handling outliers. This subtle difference in how the constraints are imposed leads to a dual form of our robust OT that can be computed efficiently for deep learning applications compared to that of the unbalanced OT dual.

We consider the ℓ_2 distance as our choice of cost function in the OT formulation. In this case, the OT distance is also called the *Wasserstein* distance. In that case, we have the following result:

Theorem 1. *Let \mathbb{P}_X and \mathbb{P}_Y be two distributions defined on a metric space. The robust Wasserstein measure admits the following dual form*

$$\begin{aligned} \mathcal{W}_{\rho_1, \rho_2}^{rob}(\mathbb{P}_X, \mathbb{P}_Y) &= \min_{\mathbb{P}_{\tilde{X}}, \mathbb{P}_{\tilde{Y}}} \max_{k \in Lip-1} \int D(x) d\mathbb{P}_{\tilde{X}} - \int D(x) d\mathbb{P}_{\tilde{Y}} \\ \text{s.t. } &\mathcal{D}_f(\mathbb{P}_{\tilde{X}} || \mathbb{P}_X) \leq \rho_1, \mathcal{D}_f(\mathbb{P}_{\tilde{Y}} || \mathbb{P}_Y) \leq \rho_2. \end{aligned} \quad (6)$$

Thus, we can obtain a dual form for robust OT similar to the *Kantorovich-Rubinstein* duality. The key difference of this dual form compared to the unbalanced OT dual (opt. (4)) is that we optimize over a single dual function $D(\cdot)$ as opposed to two dual functions in (4). This makes our formulation suited for deep learning applications such as GANs and domain adaptation. Note that the integrals in opt. (6) are taken with respect to the relaxed distributions $\mathbb{P}_{\tilde{X}}$ and $\mathbb{P}_{\tilde{Y}}$ which is a non-trivial computation.

In particular, we present two approaches for optimizing the dual problem (6):

Discrete Formulation. In practice, we observe empirical distributions $\mathbb{P}_X^{(m)}$ and $\mathbb{P}_Y^{(n)}$ from the population distributions \mathbb{P}_X and \mathbb{P}_Y , where m and n are sample sizes. Let $\{\mathbf{x}_i\}_{i=1}^m, \{\mathbf{y}_i\}_{i=1}^n$ be the samples corresponding to the empirical distribution $\mathbb{P}_X^{(m)}$ and $\mathbb{P}_Y^{(n)}$, respectively. Following [19], we use weighted empirical distribution for the perturbed distribution $\mathbb{P}_{\tilde{X}}$, i.e., $\mathbb{P}_X^{(m)}(\mathbf{x}_i) = 1/m$ and $\mathbb{P}_{\tilde{X}}(\mathbf{x}_i) = w_i^x$. Let $\mathbf{w}_x = [w_1^x, \dots, w_m^x]$. For $\mathbb{P}_{\tilde{X}}$ to be a valid pmf, \mathbf{w}_x should lie in a simplex

($\mathbf{w}^x \in \Delta^m$) i.e., $w_i^x > 0$ and $\sum_i w_i^x = 1$. Then, the robust Wasserstein objective can be written as

$$\begin{aligned} \mathcal{W}_{\rho_1, \rho_2}^{rob}(\mathbb{P}_X, \mathbb{P}_Y) &= \min_{\mathbf{w}_x \in \Delta^m, \mathbf{w}_y \in \Delta^n} \max_{\mathbf{D} \in Lip-1} (\mathbf{w}_x)^t \mathbf{d}_x - (\mathbf{w}_y)^t \mathbf{d}_y \\ &\text{s.t. } \frac{1}{m} \sum_i f(mw_i^x) \leq \rho_1, \quad \frac{1}{n} \sum_i f(nw_i^y) \leq \rho_2 \end{aligned}$$

where $\mathbf{d}_x = [\mathbf{D}(\mathbf{x}_1), \mathbf{D}(\mathbf{x}_2) \dots \mathbf{D}(\mathbf{x}_m)]$, and $\mathbf{d}_y = [\mathbf{D}(\mathbf{y}_1), \mathbf{D}(\mathbf{y}_2) \dots \mathbf{D}(\mathbf{y}_n)]$. Since $f(\cdot)$ is a convex function, the set of constraints involving \mathbf{w}_x and \mathbf{w}_y are convex w.r.t weights. We use χ^2 as our choice of f -divergence for which $f(t) = (t - 1)^2/2$. The optimization then becomes

$$\begin{aligned} \mathcal{W}_{\rho_1, \rho_2}^{rob}(\mathbb{P}_X, \mathbb{P}_Y) &= \min_{\mathbf{w}_x \in \Delta^m, \mathbf{w}_y \in \Delta^n} \max_{\mathbf{D} \in Lip-1} (\mathbf{w}_x)^t \mathbf{d}_x - (\mathbf{w}_y)^t \mathbf{d}_y \quad (7) \\ &\text{s.t. } \left\| \mathbf{w}_x - \frac{1}{m} \right\|_2 \leq \sqrt{\frac{2\rho_1}{m}}, \quad \left\| \mathbf{w}_y - \frac{1}{n} \right\|_2 \leq \sqrt{\frac{2\rho_2}{n}} \end{aligned}$$

We solve this optimization using an alternating gradient descent between \mathbf{w} and \mathbf{D} updates. The above optimization is a second-order cone program with respect to weights \mathbf{w} (for a fixed \mathbf{D}). For a fixed \mathbf{w} , \mathbf{D} is optimized using stochastic gradient descent similar to [1].

Continuous Stochastic Relaxation. In (7), weight vectors \mathbf{w}_x and \mathbf{w}_y are optimized by solving a second order cone program. Since the dimension of weight vectors is the size of the entire dataset, solving this optimization is expensive for large datasets. Hence, we propose a continuous stochastic relaxation for (6). Let us assume that supports of $\mathbb{P}_{\tilde{\mathbf{x}}}$ and \mathbb{P}_X match (satisfied in real spaces). We make the following reparameterization: $\mathbb{P}_{\tilde{\mathbf{x}}}(\mathbf{x}) = \mathbf{W}_x(\mathbf{x})\mathbb{P}_X(\mathbf{x})$. For $\mathbb{P}_{\tilde{\mathbf{x}}}$ to be a valid pdf, we require $\int \mathbf{W}_x(\mathbf{x})d\mathbb{P}_X = 1$, i.e., $\mathbb{E}_{\mathbf{x} \sim \mathbb{P}_X}[\mathbf{W}_x(\mathbf{x})] = 1$. The constraint on f -divergence becomes $\mathbb{E}_{\mathbf{x} \sim \mathbb{P}_X}[f(\mathbf{W}_x(\mathbf{x}))] \leq \rho_1$. Using these, the dual of robust Wasserstein measure can be written as

$$\begin{aligned} \mathcal{W}_{\rho_1, \rho_2}^{rob}(\mathbb{P}_X, \mathbb{P}_Y) &= \min_{\mathbf{W}_x, \mathbf{W}_y} \max_{\mathbf{D} \in Lip-1} \mathbb{E}_{\mathbf{x} \sim \mathbb{P}_X}[\mathbf{W}_x(\mathbf{x})\mathbf{D}(\mathbf{x})] - \mathbb{E}_{\mathbf{y} \sim \mathbb{P}_Y}[\mathbf{W}_y(\mathbf{y})\mathbf{D}(\mathbf{y})] \quad (8) \\ &\text{s.t. } \mathbb{E}_{\mathbf{x} \sim \mathbb{P}_X}[f(\mathbf{W}_x(\mathbf{x}))] \leq \rho_1, \quad \mathbb{E}_{\mathbf{y} \sim \mathbb{P}_Y}[f(\mathbf{W}_y(\mathbf{y}))] \leq \rho_2 \\ &\quad \mathbb{E}_{\mathbf{x} \sim \mathbb{P}_X}[\mathbf{W}_x(\mathbf{x})] = 1, \quad \mathbb{E}_{\mathbf{y} \sim \mathbb{P}_Y}[\mathbf{W}_y(\mathbf{y})] = 1, \quad \mathbf{W}_x(\mathbf{x}) \geq 0, \mathbf{W}_y(\mathbf{y}) \geq 0 \end{aligned}$$

$\mathbf{W}_x(\cdot)$ and $\mathbf{W}_y(\cdot)$ are weight functions which can be implemented using neural networks. One crucial benefit of the above formulation is that it can be easily trained using stochastic GD.

3.3 Can robust OT handle outliers?

Theorem 2. Let \mathbb{P}_X and \mathbb{P}_Y be two distributions such that \mathbb{P}_X is corrupted with γ fraction of outliers i.e., $\mathbb{P}_X = (1 - \gamma)\mathbb{P}_X^c + \gamma\mathbb{P}_X^a$, where \mathbb{P}_X^c is the clean distribution and \mathbb{P}_X^a is the outlier distribution. Let $\mathcal{W}(\mathbb{P}_X^a, \mathbb{P}_X^c) = k\mathcal{W}(\mathbb{P}_X^a, \mathbb{P}_Y)$, with $k \geq 1$. Then,

$$\mathcal{W}_{\rho, 0}^{rob}(\mathbb{P}_X, \mathbb{P}_Y) \leq \max\left(1, 1 + k\gamma - k\sqrt{2\rho\gamma(1 - \gamma)}\right)\mathcal{W}(\mathbb{P}_X^c, \mathbb{P}_Y).$$

The above theorem states that robust OT obtains a provably robust distance estimate under our outlier model. That is, the robust OT is upper bounded by a constant factor of the true Wasserstein distance. This constant depends on the hyper-parameter ρ : when ρ is appropriately chosen, robust OT measure obtains a value approximately close to the true distance. Note that we derive this result for one-sided robust OT ($\mathcal{W}_{\rho, 0}^{rob}$), which is the robust OT measure when marginals are relaxed only for one of the input distributions. This is the form we use for GANs and DA experiments (Section. 4).

Choosing ρ and the tightness of the bound: The constant ρ in our formulation is a hyper-parameter that needs to be estimated. The value of ρ denotes the extent of marginal relaxation. In applications such as GANs or domain adaptation, performance on a validation set can be used for choosing ρ . Or when the outlier fraction γ is known, an appropriate choice of ρ is $\rho = \frac{\gamma}{2(1-\gamma)}$. More details and experiments on tightness of our upper bound are provided in the Appendix.

4 Experiments

For all our experiments, we use one-sided robust Wasserstein ($\mathcal{W}_{\rho, 0}^{rob}$) where the marginals are relaxed only for one of the input distributions. Please refer to Appendix for all experimental details. Code for our experiments is available at <https://github.com/yogeshbalaji/robustOT>.

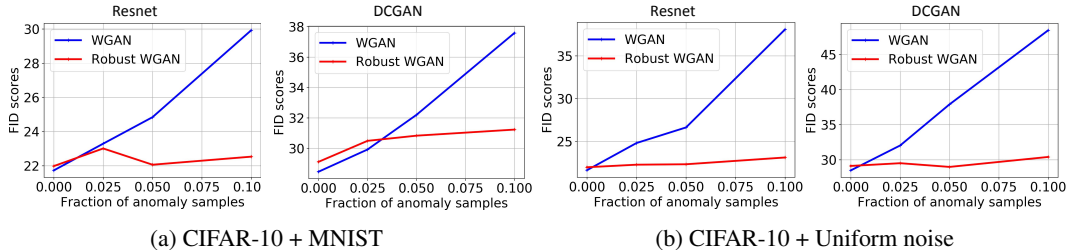


Figure 2: FID scores of GAN models trained on CIFAR-10 corrupted with outlier noise. In (a), samples from MNIST dataset are used as the outliers, while in (b), uniform noise is used. FID scores of WGAN increase with the increase in outlier fraction, while robust WGAN maintains FID scores.

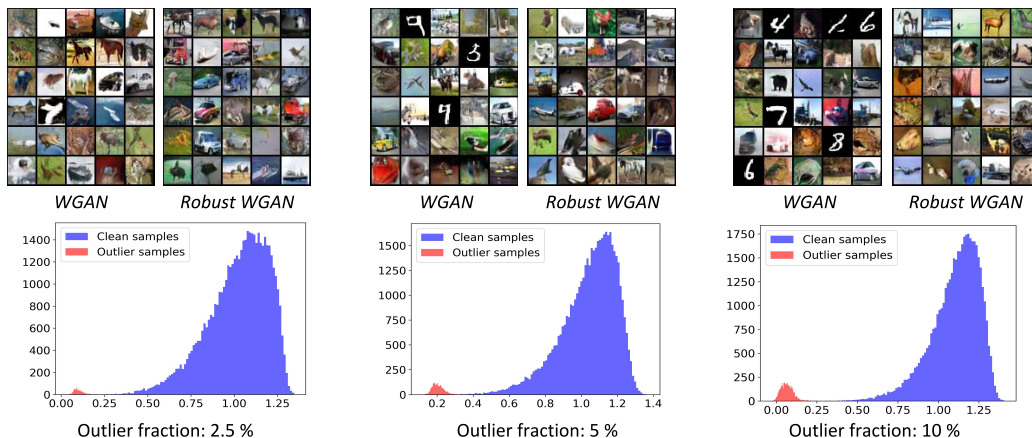


Figure 3: Visualizing samples and weight histograms. In the top panel, we show samples generated by WGAN and robust WGAN trained on CIFAR-10 dataset corrupted with MNIST samples as outliers. WGAN fits both CIFAR and MNIST samples, while robust WGAN ignores the outliers. In the bottom panel, we visualize the weights (output of the $\mathbf{W}(\cdot)$ function) for in-distribution and outlier samples. Outlier samples are assigned low weights while in-distribution samples get large weights.

4.1 Generative modeling

In this section, we show how our robust Wasserstein formulation can be used to train GANs that are insensitive to outliers. The core idea is to train a GAN by minimizing the robust Wasserstein measure (in dual form) between real and generative data distributions. Let \mathcal{G} denote a generative model which maps samples from random noise vectors to real data distribution. Using the one-directional version of the dual form of robust Wasserstein measure (8), we obtain the following optimization problem

$$\begin{aligned} \min_{\mathbf{W}, \mathcal{G}} \max_{\mathbf{D} \in Lip-1} \mathbb{E}_{\mathbf{x} \sim \mathbb{P}_X} [\mathbf{W}(\mathbf{x})\mathbf{D}(\mathbf{x})] - \mathbb{E}_{\mathbf{z}} [\mathbf{D}(\mathcal{G}(\mathbf{z}))] \\ \text{s.t. } \mathbb{E}_{\mathbf{x} \sim \mathbb{P}_X} [(\mathbf{W}(\mathbf{x}) - 1)^2] \leq 2\rho, \mathbb{E}_{\mathbf{x} \sim \mathbb{P}_X} [\mathbf{W}(\mathbf{x})] = 1, \mathbf{W}(\mathbf{x}) \geq 0 \end{aligned}$$

The first constraint is imposed using a Lagrangian term in the objective function. To impose the second constraint, we use ReLU as the final layer of $\mathbf{W}(\cdot)$ network and normalize the weights by the sum of weight vectors in a batch. This leads to the following optimization

$$\min_{\mathbf{W}, \mathcal{G}} \max_{\mathbf{D} \in Lip-1} \mathbb{E}_{\mathbf{x}} [\mathbf{W}(\mathbf{x})\mathbf{D}(\mathbf{x})] - \mathbb{E}_{\mathbf{z}} [\mathbf{D}(\mathcal{G}(\mathbf{z}))] + \lambda \max(\mathbb{E}_{\mathbf{x}} [(\mathbf{W}(\mathbf{x}) - 1)^2] - 2\rho, 0) \quad (9)$$

We set λ to a large value (typically $\lambda = 1000$) to enforce the constraint on χ^2 -divergence. A detailed algorithm can be found in Appendix. Our robust Wasserstein formulation can easily be extended to other GAN objective functions such as non-saturating loss and hinge loss, as discussed in Appendix.

Datasets with outliers: First, we train the robust Wasserstein GAN on datasets corrupted with outlier samples. For the ease of quantitative evaluation, the outlier corrupted dataset is constructed as

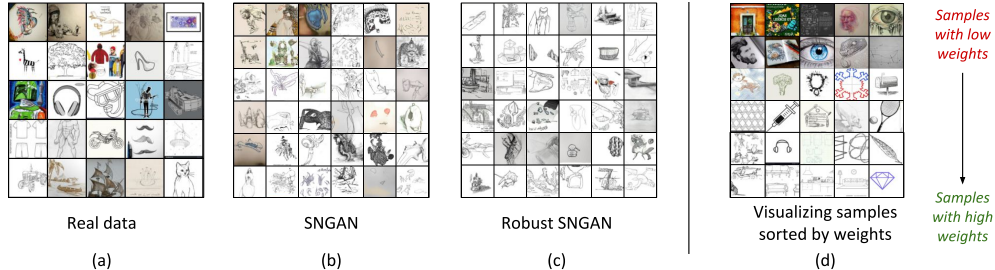


Figure 4: Visualizing samples generated on Domainnet sketch dataset. In panels (a), (b) and (c), we show the real data, samples generated by SNGAN and robust SNGAN, respectively. Robust SNGAN only generates images of sketches ignoring outliers. In panel (d), we visualize real samples sorted by weights. Low weights are assigned to outliers, while sketch images get large weights.

Table 1: Quantitative evaluation of robust WGAN on clean datasets. In each cell, the top row corresponds to the Inception score and the bottom row corresponds to the FID score.

Dataset	Arch	WGAN	RWGAN	
			$\rho = 0$	$\rho = 0.3$
CIFAR-10	DCGAN	6.86	6.84	6.91
		28.46	29.11	29.45
CIFAR-10	Resnet	7.49	7.35	7.36
		21.73	21.98	21.57
CIFAR-100	Resnet	9.01	8.79	8.93
		15.60	15.61	15.32

Table 2: Cross-domain recognition accuracy on VISDA-17 dataset using Resnet-18 model averaged over 3 runs.

Method	Accuracy (in %)
Source only	44.7
Adversarial (<i>no ent</i>)	55.4
Robust adversarial (<i>no ent</i>)	62.9
Adversarial (<i>with ent</i>)	59.5
Robust adversarial (<i>with ent</i>)	63.9

follows: We artificially add outlier samples to the CIFAR-10 dataset such they occupy γ fraction of the samples. MNIST and uniform noise are used as two choices of outlier distributions. Samples generated by Wasserstein GAN and robust Wasserstein GAN on this dataset are shown in Fig. 3. While Wasserstein GAN fits outliers in addition to the CIFAR samples, robust Wasserstein GAN effectively ignores outliers and generates samples only from the CIFAR-10 dataset.

For a quantitative evaluation, we report the FID scores of the generated samples with respect to the clean CIFAR-10 distribution (Figure 2). Since Wasserstein GAN generates outlier samples in addition to the CIFAR-10 samples, the FID scores get worse as the outlier fraction increases. Robust Wasserstein GAN, on the other hand, obtains good FID even for large fraction of outliers. This trend is consistent for both outlier distributions MNIST and uniform noise.

Next, we train our robust GAN model on a dataset where outliers are naturally present. We use *Sketch* domain of DomainNet dataset [20] for this purpose. As shown in Figure 4(a), the dataset contains many outlier samples (non-sketch images). Samples generated by spectral normalization GAN and robust spectral normalization GAN (both using Resnet) are shown in Figure 4(b, c). We observe that the SNGAN model generates some non-sketch images in addition to sketch images. Robust SNGAN, on the other hand, ignores outliers and only generates samples that look like sketches.

Clean datasets: In the previous section, we demonstrated how robust Wasserstein GAN effectively ignores outliers in the data distributions. A natural question that may arise is what would happen if one uses the robust WGAN on a clean dataset (dataset without outliers). To understand this, we train robust Wasserstein GAN on CIFAR-10 and CIFAR-100 datasets. The Inception and FID scores of generated samples are reported in Table. 1. We observe no drop in FID scores, which suggest that no modes are dropped in the generated distribution.

Usefulness of sample weights: In the optimization of the robust GAN, each sample is assigned a weight indicating the difficulty of that sample to be generated by the model. In this section, we visualize the weights learnt by our robust GAN. In Figure 3, we plot the histogram of weights assigned to in-distribution and outlier samples for robust WGAN trained on CIFAR-10 dataset corrupted with MNIST outliers. Outliers are assigned smaller weights compared to the in-distribution samples, and

Table 3: Adaptation accuracy on VISDA-17 using Resnet-50 model averaged over 3 runs

Method	Accuracy (in %)
Source Only	50.7
DAN [14]	53.0
RTN [16]	53.6
DANN [10]	55.0
JAN-A [17]	61.6
GTA [25]	69.5
SimNet [22]	69.6
CDAN-E [15]	70.0
<hr/>	
<i>Ours</i> Adversarial (<i>no ent</i>)	62.9
<i>Ours</i> Robust adversarial (<i>no ent</i>)	68.6
<i>Ours</i> Adversarial (<i>with ent</i>)	65.5
<i>Ours</i> Robust adversarial (<i>with ent</i>)	71.5

Table 4: Adaptation accuracy on VISDA-17 using Resnet-101 model averaged over 3 runs

Method	Accuracy (in %)
Source only	55.3
DAN [14]	61.1
DANN [10]	57.4
MCD [23]	71.9
<hr/>	
<i>Ours</i> Adversarial (<i>no ent</i>)	65.5
<i>Ours</i> Robust adversarial (<i>no ent</i>)	69.3
<i>Ours</i> Adversarial (<i>with ent</i>)	69.3
<i>Ours</i> Robust adversarial (<i>with ent</i>)	72.7

Table 5: Sensitivity Analysis of ρ

<i>GAN exp</i>		ρ	0	0.01	0.05	0.1	0.15
CIFAR + MNIST	FID	37.5	34.7	31.9	29.9	30.2	
	<hr/>						
<i>DA exp</i>		ρ	0.0	0.05	0.1	0.2	0.4
Resnet-18	Acc	59.5	62.8	63.1	63.9	63.6	

there is a clear separation between their corresponding histograms. For the GAN model trained on the Sketch dataset, we show a visualization of randomly chosen input samples sorted by their assigned weights in Figure 4(d). We observe that non-sketch images are assigned low weights while the true sketch images obtain larger weights. Hence, the weights learnt by our robust GAN can be a useful indicator for assessing how difficult it is to generate a given sample.

4.2 Domain adaptation

In Unsupervised Domain Adaptation (UDA) problem, we are given a labeled source dataset and an unlabeled target dataset. The source and target domains have a covariate shift i.e., the conditional distribution of the data given labels differ while the marginal distribution of labels match. Due to the covariate shift, a model trained solely on the source domain performs poorly on the target. A conventional approach for UDA involves training classification model on the source domain while minimizing a distributional distance between source and target feature distributions. Commonly used distance measures include Wasserstein distance [26] and non-saturating loss [10]. For the ease of explanation, we use Wasserstein as our choice of distance measure.

Let $\mathbb{P}_s = \{(\mathbf{x}_i^s, y_i^s)\}_{i=1}^{n_s}$ and $\mathbb{P}_t = \{(\mathbf{x}_i^t)\}_{i=1}^{n_t}$ denote the source and target distributions, respectively. Let \mathbf{F} denote a feature network, and \mathbf{C} denote a classifier. Then, the UDA optimization that minimizes the robust OT distance between source and target feature distributions can be written as

$$\min_{\mathbf{F}, \mathbf{C}} \frac{1}{n_s} \sum_i \mathcal{L}_{cls}(\mathbf{F}(\mathbf{x}_i), y_i) + \lambda \left[\min_{\mathbf{w} \in \Delta^{n_t}} \max_{\mathbf{D}} \frac{1}{n_s} \sum_i \mathbf{D}(\mathbf{F}(\mathbf{x}_i^s)) - \frac{1}{n_t} \sum_j w_j \mathbf{D}(\mathbf{F}(\mathbf{x}_j^t)) \right] \quad (10)$$

$$\text{s.t. } \|n_t \mathbf{w} - 1\|_2 \leq \sqrt{2\rho n_t}$$

where $\mathbf{w} = [w_1, w_2 \dots w_{n_t}]$. While we describe this formulation for the Wasserstein distance, similar ideas can be applied to other adversarial losses. For instance, by replacing the second and third terms of (10) with binary cross entropy loss, we obtain the non-saturating objective. Note that we use the discrete formulation of dual objective (Section 3.2) instead of the continuous one (Section 3.2). This is because in our experiments, small batch sizes (~ 28) were used due to GPU limitations. With small batch sizes, continuous relaxation gives sub-optimal performance.

For experiments, we use VISDA-17 dataset [21], which is a large scale benchmark dataset for UDA. The task is to perform 12- class classification by adapting models from synthetic to real dataset. In our experiments, we use non-saturating loss instead of Wasserstein to enable fair comparison with other adversarial approaches such as DANN. In addition to the adversarial alignment, we use an entropy regularizer on target logits, which is a standard technique used in UDA [5]. The adaptation results using Resnet-18, Resnet-50 and Resnet-101 models are shown in Tables 2, 3 and 4, respectively. Our robust adversarial objective gives consistent performance improvement of $\sim 5\%$ over the standard adversarial objective in all experiments. By using a weighted adversarial loss, our approach assigns

low weights to samples that are hard to adapt and high weights to target samples that look more similar to source, thereby promoting improved adaptation. Also, with the use of entropy regularization, our generic robust adversarial objective reaches performance on par with other competing approaches that are tuned specifically for the UDA problem. This demonstrates the effectiveness of our approach.

Ablation: Sensitivity of ρ In Table. 5, we report the sensitivity of ρ for both GANs and domain adaptation experiments. In case of GANs, performance is relatively low only for very low values of ρ and stable for higher values. For DA, sensitivity is low in general. For all DA experiments, we used $\rho = 0.2$ without tuning it individually for each setting.

5 Conclusion

In this work, we study the robust optimal transport which is insensitive to outliers (samples with large noise) in the data. The applications of previous formulations of robust OT are limited in practical deep learning problems such as GANs and domain adaptation due to the instability of their optimization solvers. In this paper, we derive a computationally efficient dual form of the robust OT objective that is suited for deep learning applications. We demonstrate the effectiveness of the proposed method in two applications of GANs and domain adaptation, where our approach is shown to effectively handle outliers and achieve good performance improvements.

6 Broader Impact

The use of optimal transport (OT) distances such as the Wasserstein distance have become increasingly popular in machine learning with several applications in generative modeling, image-to-image translation, inpainting, domain adaptation, etc. One of the shortcomings of OT is its sensitivity to input noise. Hence, using OT for large-scale machine learning problems can be problematic since noise in large datasets is inevitable. Building on theoretical formulations of unbalanced OT which suffer from computational instability in deep learning applications, we have developed an efficient learning method that is provably robust against outliers and is amenable to complex deep learning applications such as deep generative modeling and domain adaptation. These attributes ensure broader impacts of this work in both theoretical and applied machine learning communities and can act as a bridge between the two. To the best of our knowledge, this work does not lead to any negative outcomes either in ethical or societal aspects.

7 Acknowledgements

This project was supported in part by NSF CAREER AWARD 1942230, a Simons Fellowship on Deep Learning Foundations, and a MURI program from the Army Research Office under the grant W911NF17-1-0304.

References

- [1] Martin Arjovsky, Soumith Chintala, and Léon Bottou. Wasserstein generative adversarial networks. In *Proceedings of the 34th International Conference on Machine Learning, ICML 2017, Sydney, Australia, 7-9 August, 2017*, 2017.
- [2] Yogesh Balaji, Rama Chellappa, and Soheil Feizi. Normalized wasserstein for mixture distributions with applications in adversarial learning and domain adaptation. In *The IEEE International Conference on Computer Vision (ICCV)*, October 2019.
- [3] Jean-David Benamou, Guillaume Carlier, Marco Cuturi, Luca Nenna, and Gabriel Peyré. Iterative bregman projections for regularized transportation problems. *SIAM Journal on Scientific Computing*, 2015.
- [4] Nicolas Bonneel, Gabriel Peyré, and Marco Cuturi. Wasserstein Barycentric Coordinates: Histogram Regression Using Optimal Transport. *ACM Transactions on Graphics (SIGGRAPH 2016)*, 35(4), 2016.

- [5] Fabio Maria Carlucci, Lorenzo Porzi, Barbara Caputo, Elisa Ricci, and Samuel Rota Buló. Autodial: Automatic domain alignment layers. In *International Conference on Computer Vision (ICCV)*, 2017.
- [6] Lenaïc Chizat, Gabriel Peyré, Bernhard Schmitzer, and François-Xavier Vialard. Unbalanced optimal transport: Dynamic and Kantorovich formulation. *arXiv preprint arXiv:1508.05216*, 2015.
- [7] Lenaïc Chizat, Gabriel Peyré, Bernhard Schmitzer, and François-Xavier Vialard. Scaling algorithms for unbalanced transport problems. *arXiv preprint arXiv:1607.05816*, 2016.
- [8] Marco Cuturi. Sinkhorn distances: Lightspeed computation of optimal transport. In C. J. C. Burges, L. Bottou, M. Welling, Z. Ghahramani, and K. Q. Weinberger, editors, *Advances in Neural Information Processing Systems 26*, pages 2292–2300. Curran Associates, Inc., 2013.
- [9] Charlie Frogner, Chiyuan Zhang, Hossein Mobahi, Mauricio Araya, and Tomaso A Poggio. Learning with a Wasserstein loss. In *Advances in Neural Information Processing Systems*, pages 2053–2061, 2015.
- [10] Yaroslav Ganin and Victor Lempitsky. Unsupervised domain adaptation by backpropagation. In Francis Bach and David Blei, editors, *Proceedings of the 32nd International Conference on Machine Learning*, volume 37 of *Proceedings of Machine Learning Research*, pages 1180–1189, Lille, France, 07–09 Jul 2015. PMLR.
- [11] Ishaan Gulrajani, Faruk Ahmed, Martin Arjovsky, Vincent Dumoulin, and Aaron C Courville. Improved training of Wasserstein GANs. In I. Guyon, U. V. Luxburg, S. Bengio, H. Wallach, R. Fergus, S. Vishwanathan, and R. Garnett, editors, *Advances in Neural Information Processing Systems 30*, pages 5767–5777. Curran Associates, Inc., 2017.
- [12] Stanislav Kondratyev, Léonard Monsaingeon, Dmitry Vorotnikov, et al. A new optimal transport distance on the space of finite Radon measures. *Advances in Differential Equations*, 21(11/12):1117–1164, 2016.
- [13] Matthias Liero, Alexander Mielke, and Giuseppe Savaré. Optimal entropy-transport problems and a new Hellinger–Kantorovich distance between positive measures. *Inventiones mathematicae*, 211(3):969–1117, Mar 2018.
- [14] Mingsheng Long, Yue Cao, Jianmin Wang, and Michael I. Jordan. Learning transferable features with deep adaptation networks. In *Proceedings of the 32nd International Conference on Machine Learning*, pages 97–105, 2015.
- [15] Mingsheng Long, ZHANGJIE CAO, Jianmin Wang, and Michael I Jordan. Conditional adversarial domain adaptation. In S. Bengio, H. Wallach, H. Larochelle, K. Grauman, N. Cesa-Bianchi, and R. Garnett, editors, *Advances in Neural Information Processing Systems 31*, pages 1640–1650. Curran Associates, Inc., 2018.
- [16] Mingsheng Long, Jianmin Wang, and Michael I. Jordan. Unsupervised domain adaptation with residual transfer networks. *CoRR*, abs/1602.04433, 2016.
- [17] Mingsheng Long, Han Zhu, Jianmin Wang, and Michael I. Jordan. Deep transfer learning with joint adaptation networks. In Doina Precup and Yee Whye Teh, editors, *Proceedings of the 34th International Conference on Machine Learning, ICML 2017, Sydney, NSW, Australia, 6-11 August 2017*, volume 70 of *Proceedings of Machine Learning Research*, pages 2208–2217. PMLR, 2017.
- [18] Takeru Miyato and Masanori Koyama. cGANs with projection discriminator. In *International Conference on Learning Representations*, 2018.
- [19] Hongseok Namkoong and John C Duchi. Stochastic gradient methods for distributionally robust optimization with f-divergences. In D. D. Lee, M. Sugiyama, U. V. Luxburg, I. Guyon, and R. Garnett, editors, *Advances in Neural Information Processing Systems 29*, pages 2208–2216. Curran Associates, Inc., 2016.
- [20] Xingchao Peng, Qinxun Bai, Xide Xia, Zijun Huang, Kate Saenko, and Bo Wang. Moment matching for multi-source domain adaptation. *arXiv preprint arXiv:1812.01754*, 2018.
- [21] Xingchao Peng, Ben Usman, Neela Kaushik, Judy Hoffman, Dequan Wang, and Kate Saenko. Visda: The visual domain adaptation challenge. *CoRR*, abs/1710.06924, 2017.
- [22] Pedro Oliveira Pinheiro. Unsupervised domain adaptation with similarity learning. *CoRR*, abs/1711.08995, 2017.

- [23] Kuniaki Saito, Kohei Watanabe, Yoshitaka Ushiku, and Tatsuya Harada. Maximum classifier discrepancy for unsupervised domain adaptation. *arXiv preprint arXiv:1712.02560*, 2017.
- [24] Maziar Sanjabi, Jimmy Ba, Meisam Razaviyayn, and Jason D Lee. On the convergence and robustness of training gans with regularized optimal transport. In S. Bengio, H. Wallach, H. Larochelle, K. Grauman, N. Cesa-Bianchi, and R. Garnett, editors, *Advances in Neural Information Processing Systems 31*, pages 7091–7101. Curran Associates, Inc., 2018.
- [25] Swami Sankaranarayanan, Yogesh Balaji, Carlos D. Castillo, and Rama Chellappa. Generate to adapt: Aligning domains using generative adversarial networks. In *The IEEE Conference on Computer Vision and Pattern Recognition (CVPR)*, June 2018.
- [26] Jian Shen, Yanru Qu, Weinan Zhang, and Yong Yu. Wasserstein distance guided representation learning for domain adaptation. In *AAAI*, pages 4058–4065. AAAI Press, 2018.
- [27] Justin Solomon, Fernando de Goes, Gabriel Peyré, Marco Cuturi, Adrian Butscher, Andy Nguyen, Tao Du, and Leonidas J. Guibas. Convolutional wasserstein distances: efficient optimal transportation on geometric domains. *ACM Trans. Graph.*, 34(4):66:1–66:11, 2015.
- [28] Justin Solomon, Raif M. Rustamov, Leonidas J. Guibas, and Adrian Butscher. Wasserstein propagation for semi-supervised learning. In *ICML*, volume 32 of *JMLR Workshop and Conference Proceedings*, pages 306–314. JMLR.org, 2014.
- [29] Cédric Villani. *Optimal transport: old and new*, volume 338. Springer Science & Business Media, 2008.
- [30] Karren D. Yang and Caroline Uhler. Scalable unbalanced optimal transport using generative adversarial networks. In *International Conference on Learning Representations*, 2019.

A Proofs

In this section, we present the proofs:

Duality:

Theorem 3. *Let \mathbb{P}_X and \mathbb{P}_Y be two distributions defined on a metric space. The robust Wasserstein measure admits the following dual form*

$$\begin{aligned} \mathcal{W}_{\rho_1, \rho_2}^{rob}(\mathbb{P}_X, \mathbb{P}_Y) &= \min_{\mathbb{P}_{\tilde{X}}, \mathbb{P}_{\tilde{Y}}} \max_{k \in Lip-1} \int D(x) d\mathbb{P}_{\tilde{X}} - \int D(x) d\mathbb{P}_{\tilde{Y}} \\ &\text{s.t. } \mathcal{D}_f(\mathbb{P}_{\tilde{X}} || \mathbb{P}_X) \leq \rho_1, \mathcal{D}_f(\mathbb{P}_{\tilde{Y}} || \mathbb{P}_Y) \leq \rho_2. \end{aligned} \quad (11)$$

Proof: We begin with the primal form of the robust optimal transport defined as

$$\begin{aligned} \mathcal{W}_{\rho_1, \rho_2}^{rob}(\mathbb{P}_X, \mathbb{P}_Y) &= \min_{\mathbb{P}_{\tilde{X}}, \mathbb{P}_{\tilde{Y}} \in Prob(\mathcal{X})} \min_{\pi} \int \int c(x, y) \pi(x, y) dx dy \\ &\text{s.t. } \mathcal{D}_f(\mathbb{P}_{\tilde{X}} || \mathbb{P}_X) \leq \rho_1, \mathcal{D}_f(\mathbb{P}_{\tilde{Y}} || \mathbb{P}_Y) \leq \rho_2 \\ &\int \pi(x, y) dy = \mathbb{P}_{\tilde{X}}, \int \pi(x, y) dx = \mathbb{P}_{\tilde{Y}} \end{aligned}$$

The constraint $\mathbb{P}_{\tilde{X}}, \mathbb{P}_{\tilde{Y}} \in Prob(\mathcal{X})$ states that $\mathbb{P}_{\tilde{X}}$ and $\mathbb{P}_{\tilde{Y}}$ are valid probability distributions. For brevity, we shall ignore explicitly stating it in the rest of the proof. Now, we write the Lagrangian function with respect to marginal constraints.

$$\begin{aligned} L &= \min_{\mathbb{P}_{\tilde{X}}, \mathbb{P}_{\tilde{Y}}} \min_{\pi > 0} \max_{\phi(x), \psi(y)} \int \int c(x, y) \pi(x, y) dx dy + \int \phi(x) \left(\int \mathbb{P}_{\tilde{X}} - \pi(x, y) dy \right) dx \\ &\quad + \int \psi(y) \left(\int \pi(x, y) dx - \mathbb{P}_{\tilde{Y}} \right) dy \\ &\text{s.t. } \mathcal{D}_f(\mathbb{P}_{\tilde{X}} || \mathbb{P}_X) \leq \rho_1, \mathcal{D}_f(\mathbb{P}_{\tilde{Y}} || \mathbb{P}_Y) \leq \rho_2 \\ &= \min_{\mathbb{P}_{\tilde{X}}, \mathbb{P}_{\tilde{Y}}} \min_{\pi > 0} \max_{\phi(x), \psi(y)} \int \int [c(x, y) - \phi(x) + \psi(y)] \pi(x, y) dx dy + \int \phi(x) d\mathbb{P}_{\tilde{X}} - \int \psi(y) d\mathbb{P}_{\tilde{Y}} \\ &\text{s.t. } \mathcal{D}_f(\mathbb{P}_{\tilde{X}} || \mathbb{P}_X) \leq \rho_1, \mathcal{D}_f(\mathbb{P}_{\tilde{Y}} || \mathbb{P}_Y) \leq \rho_2 \end{aligned}$$

Since $\pi > 0$, we observe that

$$c(x, y) - \phi(x) + \psi(y) = \begin{cases} \infty & \text{if } c(x, y) - \phi(x) + \psi(y) > 0 \\ 0 & \text{otherwise} \end{cases}$$

Hence, the dual formulation becomes

$$\begin{aligned} \mathcal{W}_{\rho_1, \rho_2}^{rob}(\mathbb{P}_X, \mathbb{P}_Y) &= \min_{\mathbb{P}_{\tilde{X}}, \mathbb{P}_{\tilde{Y}}} \max_{\phi(x), \psi(y)} \int \phi(x) d\mathbb{P}_{\tilde{X}} - \int \psi(y) d\mathbb{P}_{\tilde{Y}} \\ &\text{s.t. } \phi(x) - \psi(y) \leq c(x, y) \\ &\mathcal{D}_f(\mathbb{P}_{\tilde{X}} || \mathbb{P}_X) \leq \rho_1, \mathcal{D}_f(\mathbb{P}_{\tilde{Y}} || \mathbb{P}_Y) \leq \rho_2 \end{aligned} \quad (12)$$

Furthermore, when the distributions lie in a metric space, we can further simplify this duality. Define

$$k(x) := \inf_y c(x, y) + \psi(y) \quad (13)$$

Since the feasible set in the dual problem satisfies $\phi(x) - \psi(y) \leq c(x, y)$, $\phi(x) \leq k(x)$, and by using $y = x$ in Eq (13), we obtain, $k(x) \leq \psi(x)$. Hence, $\phi(x) \leq k(x) \leq \psi(x)$.

$$\begin{aligned} |k(x) - k(x')| &= \left| \inf_y [c(x, y) + \psi(y)] - \inf_y [c(x', y) + \psi(y)] \right| \\ &\leq |c(x, y) - c(x', y)| \end{aligned}$$

Hence, $k(\cdot)$ is 1-Lipschitz. Using the above inequalities in (12), we obtain,

$$\begin{aligned} \mathcal{W}_{\rho_1, \rho_2}^{rob}(\mathbb{P}_X, \mathbb{P}_Y) &\leq \min_{\mathbb{P}_{\tilde{X}}, \mathbb{P}_{\tilde{Y}}} \max_{k \in Lip-1} \int k(x) d\mathbb{P}_{\tilde{X}} - \int k(x) d\mathbb{P}_{\tilde{Y}} \\ &\text{s.t. } \mathcal{D}_f(\mathbb{P}_{\tilde{X}} \| \mathbb{P}_X) \leq \rho_1, \mathcal{D}_f(\mathbb{P}_{\tilde{Y}} \| \mathbb{P}_Y) \leq \rho_2 \end{aligned}$$

Also, $\phi(x) = k(x)$ and $\psi(x) = k(x)$ is a feasible solution in optimization (12). Since (12) maximizes over $\phi(\cdot)$ and $\psi(\cdot)$, we obtain

$$\begin{aligned} \mathcal{W}_{\rho_1, \rho_2}^{rob}(\mathbb{P}_X, \mathbb{P}_Y) &\geq \min_{\mathbb{P}_{\tilde{X}}, \mathbb{P}_{\tilde{Y}}} \max_{k \in Lip-1} \int k(x) d\mathbb{P}_{\tilde{X}} - \int k(x) d\mathbb{P}_{\tilde{Y}} \\ &\text{s.t. } \mathcal{D}_f(\mathbb{P}_X, \mathbb{P}_{\tilde{X}}) \leq \rho_1, \mathcal{D}_f(\mathbb{P}_Y, \mathbb{P}_{\tilde{Y}}) \leq \rho_2 \end{aligned}$$

Combining these two inequalities, we obtain

$$\begin{aligned} \mathcal{W}_{\rho_1, \rho_2}^{rob}(\mathbb{P}_X, \mathbb{P}_Y) &= \min_{\mathbb{P}_{\tilde{X}}, \mathbb{P}_{\tilde{Y}}} \max_{k \in Lip-1} \int k(x) d\mathbb{P}_{\tilde{X}} - \int k(x) d\mathbb{P}_{\tilde{Y}} \\ &\text{s.t. } \mathcal{D}_f(\mathbb{P}_X, \mathbb{P}_{\tilde{X}}) \leq \rho_1, \mathcal{D}_f(\mathbb{P}_Y, \mathbb{P}_{\tilde{Y}}) \leq \rho_2 \end{aligned} \quad (14)$$

The above equation is similar in spirit to the *Kantorovich-Rubinstein* duality. An important observation to note is that the above optimization only maximizes over a single discriminator function (as opposed to two functions in optimization (12)). Hence, it is easier to train it in large-scale deep learning problems such as GANs.

Provable robustness:

Theorem 4. Let \mathbb{P}_X and \mathbb{P}_Y be two distributions such that \mathbb{P}_X is corrupted with γ fraction of outliers i.e., $\mathbb{P}_X = (1 - \gamma)\mathbb{P}_X^c + \gamma\mathbb{P}_X^a$, where \mathbb{P}_X^c is the clean distribution and \mathbb{P}_X^a is the outlier distribution. Let $\mathcal{W}(\mathbb{P}_X^a, \mathbb{P}_X^c) = k\mathcal{W}(\mathbb{P}_X^c, \mathbb{P}_Y)$, with $k \geq 1$. Then,

$$\mathcal{W}_{\rho, 0}^{rob}(\mathbb{P}_X, \mathbb{P}_Y) \leq \max\left(1, 1 + k\gamma - k\sqrt{2\rho\gamma(1 - \gamma)}\right)\mathcal{W}(\mathbb{P}_X^c, \mathbb{P}_Y).$$

Proof: We consider the case of empirical distributions. Let $\{\mathbf{x}_i^a\}_{i=1}^{n_a}$ be the samples in the anomaly distribution \mathbb{P}_X^a , $\{\mathbf{x}_i^c\}_{i=1}^{n_c}$ be the samples in the clean distribution \mathbb{P}_X^c , and $\{\mathbf{y}_i\}_{i=1}^m$ be the samples in the distribution \mathbb{P}_Y . We also know that $\frac{n_a}{n_a + n_c} = \gamma$.

$\mathcal{W}_{\rho, 0}^{rob}(\mathbb{P}_X, \mathbb{P}_Y)$ is defined as

$$\begin{aligned} \mathcal{W}_{\rho, 0}^{rob}(\mathbb{P}_X, \mathbb{P}_Y) &= \min_{\mathbb{P}_{\tilde{X}} \in Prob(\mathcal{X})} \min_{\pi} \sum_i \sum_j \pi_{ij} c_{ij} \\ &\text{s.t. } \sum_j \pi_{ij} = \mathbb{P}_{\tilde{X}}, \sum_i \pi_{ij} = \mathbb{P}_Y, \mathcal{D}_{\chi^2}(\mathbb{P}_{\tilde{X}} \| \mathbb{P}_X) \leq \rho \end{aligned}$$

Let π^{c*} and π^{a*} be the optimal transport plans for $\mathcal{W}(\mathbb{P}_X^c, \mathbb{P}_Y)$ and $\mathcal{W}(\mathbb{P}_X^a, \mathbb{P}_Y)$ respectively. We consider transport plans of the form $\beta\pi^{a*} + (1 - \beta)\pi^{c*}$, for $\beta \in [0, 1]$. The marginal constraints can then be written as

$$\begin{aligned} \int \beta\pi^{a*} + (1 - \beta)\pi^{c*} dx &= \beta\mathbb{P}_X^a + (1 - \beta)\mathbb{P}_X^c \\ \int \beta\pi^{a*} + (1 - \beta)\pi^{c*} dy &= \mathbb{P}_Y \end{aligned}$$

For this to be a feasible solution for $\mathcal{W}_{\rho, 0}^{rob}(\mathbb{P}_X, \mathbb{P}_Y)$, we require

$$\mathcal{D}_{\chi^2}(\beta\mathbb{P}_X^a + (1 - \beta)\mathbb{P}_X^c \| \gamma\mathbb{P}_X^a + (1 - \gamma)\mathbb{P}_X^c) \leq \rho$$

The distribution $\beta\mathbb{P}_X^a + (1 - \beta)\mathbb{P}_X^c$ can be characterized as

$$\left[\underbrace{\frac{\beta}{n_a}, \dots}_{n_a \text{ terms}}, \underbrace{\frac{1 - \beta}{n_c}, \dots}_{n_c \text{ terms}} \right].$$

Using this, the above constraint can be written as

$$(\beta - \gamma)^2 \leq 2\rho\gamma(1 - \gamma) \quad (15)$$

Hence, all transport plans of the form $\beta\pi^{a*} + (1 - \beta)\pi^{c*}$ are feasible solutions of $\mathcal{W}_{\rho,0}^{rob}(\mathbb{P}_X, \mathbb{P}_Y)$ if β satisfies $(\beta - \gamma)^2 \leq 2\rho\gamma(1 - \gamma)$. Therefore, we have:

$$\begin{aligned} \mathcal{W}_{\rho,0}^{rob}(\mathbb{P}_X, \mathbb{P}_Y) &\leq \min_{\beta} \sum_i \sum_j c_{i,j} [\beta\pi_{i,j}^{a*} + (1 - \beta)\pi_{i,j}^{c*}] \\ &\leq \min_{\beta} \beta\mathcal{W}(\mathbb{P}_X^a, \mathbb{P}_Y) + (1 - \beta)\mathcal{W}(\mathbb{P}_X^c, \mathbb{P}_Y) \\ &\text{s.t. } (\beta - \gamma)^2 \leq 2\rho\gamma(1 - \gamma) \end{aligned}$$

By the assumption, we have:

$$\begin{aligned} \mathcal{W}(\mathbb{P}_X^c, \mathbb{P}_X^a) &= k\mathcal{W}(\mathbb{P}_X^c, \mathbb{P}_Y) \\ \mathcal{W}(\mathbb{P}_X^a, \mathbb{P}_Y) &\leq \mathcal{W}(\mathbb{P}_X^a, \mathbb{P}_X^c) + \mathcal{W}(\mathbb{P}_X^c, \mathbb{P}_Y) \\ &\leq (k + 1)\mathcal{W}(\mathbb{P}_X^c, \mathbb{P}_Y) \end{aligned}$$

Hence,

$$\begin{aligned} \mathcal{W}_{\rho,0}^{rob}(\mathbb{P}_X, \mathbb{P}_Y) &\leq \min_{\beta} (1 + \beta k)\mathcal{W}(\mathbb{P}_X^c, \mathbb{P}_Y) \\ &\text{s.t. } (\beta - \gamma)^2 \leq 2\rho\gamma(1 - \gamma) \end{aligned}$$

The smallest value β can take is $\gamma - \sqrt{2\rho\gamma(1 - \gamma)}$. This gives

$$\mathcal{W}_{\rho,0}^{rob}(\mathbb{P}_X, \mathbb{P}_Y) \leq \max\left(1, 1 + k\gamma - k\sqrt{2\rho\gamma(1 - \gamma)}\right)\mathcal{W}(\mathbb{P}_X^c, \mathbb{P}_Y)$$

Note: The transport plan $\beta\pi^{a*} + (1 - \beta)\pi^{c*}$ is not the the optimal transport plan for the robust OT optimization between corrupted distribution \mathbb{P}_X and \mathbb{P}_Y . However, this plan is a ‘‘feasible’’ solution that satisfies the constraints of the robust OT. Hence, the cost obtained by this plan is an upper bound to the true robust OT cost.

B Practical Issues with Unbalanced Optimal Transport Dual

B.1 Dual Objective

The primal form of unbalanced OT [13, 6] is given by

$$\mathcal{W}^{ub}(\mathbb{P}_X, \mathbb{P}_Y) = \min_{\pi \in \Pi(\mathbb{P}_X, \mathbb{P}_Y)} \int c(x, y)\pi(x, y)dxdy + \mathcal{D}_f(\mathbb{P}_{\tilde{X}}||\mathbb{P}_X) + \mathcal{D}_f(\mathbb{P}_{\tilde{Y}}||\mathbb{P}_Y) \quad (16)$$

where \mathcal{D}_f is the f -divergence between distributions, defined as $\mathcal{D}_f(P||Q) = \int f\left(\frac{dP}{dQ}\right)dQ$. Furthermore, the authors of [13] derived a dual form for the problem. Let f be a convex lower semi-continuous function. Define $r^*(x) := \sup_{s>0} \frac{x-f(s)}{s}$ where $f'_\infty := \lim_{s \rightarrow \infty} \frac{f(s)}{s}$. Then,

$$\begin{aligned} \mathcal{W}^{ub}(\mathbb{P}_X, \mathbb{P}_Y) &= \max_{\phi, \psi} \int \phi(x)d\mathbb{P}_X + \int \psi(y)d\mathbb{P}_Y \\ &\text{s.t. } r^*(\phi(x)) + r^*(\psi(y)) \leq c(x, y) \end{aligned} \quad (17)$$

In our case, $f(x) = (x - 1)^2/2$. Let us now, write the dual for this case. First, we need to find $r^*(x)$ for this function.

$$\begin{aligned} r^*(x) &= \sup_{s>0} \frac{x - f(s)}{s} \\ &= \sup_{s>0} \frac{x - (s - 1)^2/2}{s} \\ &= \sup_{s>0} \frac{2x - 1 - s^2 + 2s}{2s} \\ &= \sup_{s>0} \frac{2x - 1}{2s} - \frac{s}{2} + 1 \end{aligned}$$

We consider three cases:

Case 1: $x > 1/2$. In this case, $r^*(x) \rightarrow \infty$ as $s \rightarrow 0^+$.

Case 2: $x = 1/2$. In this case, $r^*(x) = 1$.

Case 3: $x < 1/2$. In this case, for $s \rightarrow 0^+$, $r^*(x) \rightarrow -\infty$. Also, when $s \rightarrow \infty$, $r^*(x) \rightarrow -\infty$. So, the maximizer has to lie somewhere in $(0, \infty)$.

Taking the derivative w.r.t. s , we obtain,

$$\frac{1-2x}{2s^2} - \frac{1}{2} = 0$$

This gives

$$s = \sqrt{1-2x}$$

The second derivative is also negative at this point. Hence, it is the maximizer point. Substituting this in $r^*(\cdot)$, we obtain

$$r^*(x) = 1 - \sqrt{1-2x}$$

This gives the solution,

$$r^*(x) = \begin{cases} \infty & x > 1/2 \\ 1 - \sqrt{1-2x} & x \leq 1/2 \end{cases}$$

Hence, the dual form becomes

$$\begin{aligned} \mathcal{W}^{ub}(\mathbb{P}_X, \mathbb{P}_Y) &= \max_{\phi, \psi} \int \phi(x) d\mathbb{P}_X + \int \psi(y) d\mathbb{P}_Y \\ \text{s.t. } &1 - \sqrt{1-2\phi(x)} + 1 - \sqrt{1-2\psi(y)} \leq c(x, y) \\ &\phi(x) \leq 1/2, \quad \psi(y) \leq 1/2 \end{aligned} \quad (18)$$

B.2 Practical Implementation and Training Issues

To simplify notation, we make a substitution $\mathbf{D}_1(x) \leftarrow 2\phi(x)$ and $\mathbf{D}_2(x) \leftarrow 2\psi(x)$ in (18). This gives

$$\begin{aligned} \mathcal{W}^{ub}(\mathbb{P}_X, \mathbb{P}_Y) &= \max_{\mathbf{D}_1, \mathbf{D}_2} \int \mathbf{D}_1(x) d\mathbb{P}_X + \int \mathbf{D}_2(y) d\mathbb{P}_Y \\ \text{s.t. } &1 - \sqrt{1-\mathbf{D}_1(x)} + 1 - \sqrt{1-\mathbf{D}_2(y)} \leq c(x, y) \\ &\mathbf{D}_1(x) \leq 1, \quad \mathbf{D}_2(y) \leq 1 \end{aligned} \quad (19)$$

Then, the second set of constraints (i.e. $\mathbf{D}_1(x)$ and $\mathbf{D}_2(y)$ to be less or equal to one) can be integrated into the network design. The first constraint can be implemented using a Lagrangian constraint. This leads us to the following objective:

$$\begin{aligned} \min_{\mathbf{G}} \max_{\mathbf{D}_1, \mathbf{D}_2 \leq 1} & \mathbb{E}_{\mathbf{x} \sim p_{data}} \mathbf{D}_1(\mathbf{x}) + \mathbb{E}_{\mathbf{z} \sim p_z} \mathbf{D}_2(\mathbf{G}(\mathbf{z})) \\ & - \lambda \mathbb{E}_{\mathbf{x}, \mathbf{z}} \left[\max \left(\sqrt{1-\mathbf{D}_1(\mathbf{x})} + \sqrt{1-\mathbf{D}_2(\mathbf{G}(\mathbf{z}))} + c(\mathbf{x}, \mathbf{G}(\mathbf{z})) - 2, 0 \right) \right] \end{aligned} \quad (20)$$

The constraint $\mathbf{D}_1, \mathbf{D}_2 \leq 1$ means $\mathbf{D}_1(\mathbf{x}) \leq 1, \mathbf{D}_2(\mathbf{x}) \leq 1, \forall \mathbf{x}$. We trained a model using this dual objective on CIFAR-10 dataset using Resnet architecture for generator and discriminator network. However, partially due to the presence of two discriminator networks \mathbf{D}_1 and \mathbf{D}_2 , the training is challenging. Similar training difficulties in GANs with multiple discriminator networks have been observed in [24]. Even with a sweep of hyper-parameters, we were not able to make the model based on optimization 20 to converge to a proper solution.

Training loss curves of our model vs. that of unbalanced OT are shown in Figure. 5. Samples generated by our dual and unbalanced OT dual is shown in Figure. 6. We observe that the model trained using the Unbalanced OT dual produces loss curve that is flat and does not learn a proper solution. This is also evident from Figure. 6. Models trained using our dual generates CIFAR-like samples, while the one trained with unbalanced OT dual produces noisy images.

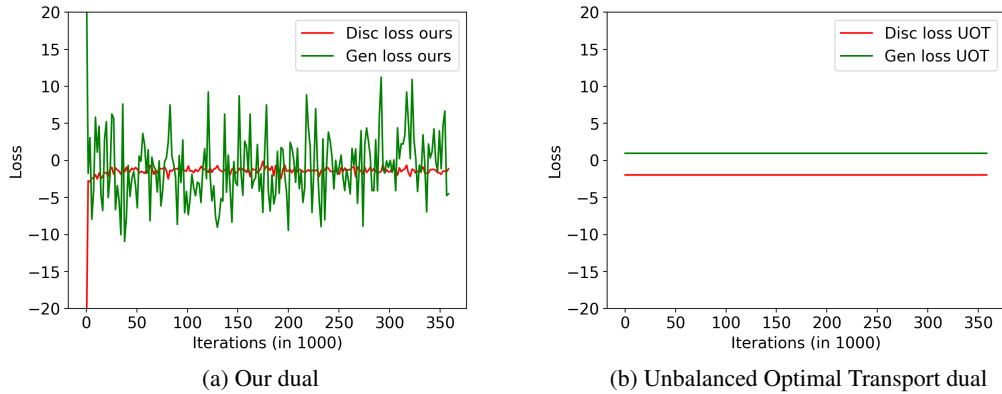


Figure 5: Loss curves of training GANs using practical implementations of our proposed dual vs. the dual of Unbalanced OT. Our model converges to a proper solution while the model trained using the dual of unbalanced OT does not converge to a good solution.

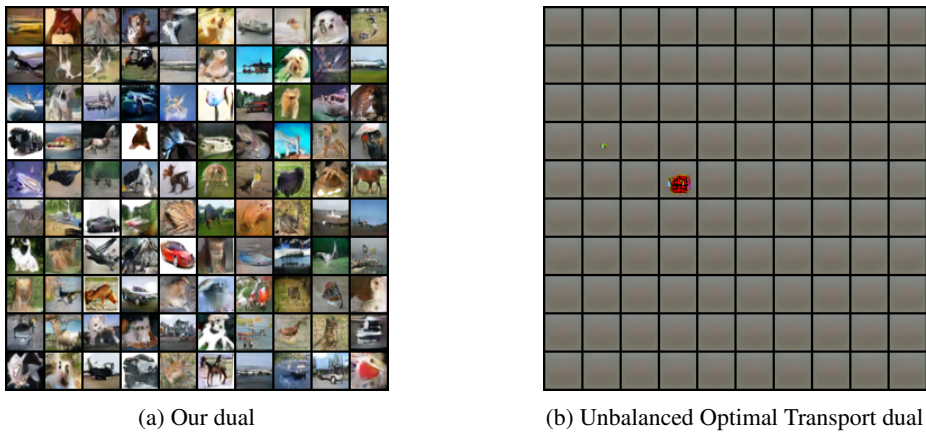


Figure 6: Samples generated by our dual and Unbalanced OT dual.

C Choosing ρ and the tightness of the bound

The constant ρ in our formulation is a hyper-parameter that needs to be estimated. The value of ρ denotes the extent of marginal relaxation. In applications such as GANs or domain adaptation, performance on a validation set can be used for choosing ρ . In the absence of validation set, we present two techniques for estimating ρ .

When outlier fraction is known: When the outlier fraction γ is known, a good estimate of ρ is $\rho = \gamma/2(1 - \gamma)$. Below we explain this claim.

Ideally, we desire the perturbed distribution $\mathbb{P}_{\tilde{X}}$ to be such that

$$\mathbb{P}_{\tilde{X}} = [\underbrace{\kappa, \kappa, \dots, \kappa}_{\text{normal samples}}, \underbrace{0, 0, \dots, 0}_{\text{outlier samples}}].$$

Since the outlier fraction is γ , the number of normal samples is $(1 - \gamma)n$ and the number of outlier samples is γn . For $\mathbb{P}_{\tilde{X}}$ to be a valid pmf, we require,

$$\begin{aligned} \kappa(1 - \gamma)n &= 1 \\ \kappa &= \frac{1}{(1 - \gamma)n} \end{aligned}$$

Also, we have a constraint on f -divergence to ensure $\mathcal{D}_{\chi^2}(\mathbb{P}_{\tilde{X}}||\mathbb{P}_X) \leq \rho$. This condition simplifies to

$$\frac{1}{2} \left[\frac{(\alpha - 1/n)^2}{1/n} (1 - \gamma)n + \frac{(0 - 1/n)^2}{1/n} \gamma n \right] \leq \rho$$

Therefore, we obtain

$$\rho \geq \frac{\gamma}{1 - \gamma}$$

Hence, to get a proper estimate of the robust Wasserstein distance, we choose $\rho = \gamma/2(1 - \gamma)$. Note that by substituting $\rho = \gamma/2(1 - \gamma)$ in Theorem 1, we obtain, $\mathcal{W}_{\rho,0}^{rob}(\mathbb{P}_X, \mathbb{P}_Y) \leq \mathcal{W}(\mathbb{P}_X, \mathbb{P}_Y)$.

Heuristic: In general, estimating ρ is non-trivial. We now present a heuristic that can be used for this purpose. First, we compute robust OT measure for various values of ρ . This curve has an elbow shape, and its point of inflection can be used as an estimate of ρ . We demonstrate this with an example. We use the mixture of four Gaussians datasets as shown in Figure 1 of the main paper as our input distributions. The means of the Gaussians are placed in a circumference of a circle, with two distributions being the rotated versions of each other. We introduce 5% outlier samples in one distribution. A plot of robust Wasserstein measure varying ρ is shown in Fig. 7 (in blue). We observe that initially as ρ increases, the robust OT value decreases sharply followed by a gradual descent, resembling the pattern of the elbow curve in k -means clustering. The point of inflection in this elbow curve is a proper estimate of ρ .

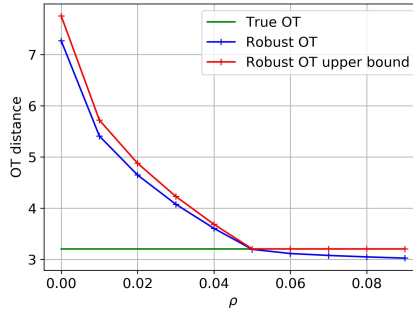


Figure 7: Plot of robust OT estimate for different values of ρ

Tightness of the upper bound: In Figure. 7, we plot the upper bound of the robust OT estimate as given by Theorem 4 in red. We observe that the upper bound is fairly tight in this case. It closely approximates the true robust OT measure given by the blue curve.

Table 6: **Analyzing mode drop:** Training robust GAN on imbalanced CelebA. Each column denotes an experiment where GAN models are trained on input dataset having the respective fraction of males as given in row 1. Rows 2 and 3 denote the fraction of males in the generated dataset obtained by training Vanilla and Robust GAN respectively. We observe that images of males are generated even when the fraction of males in the input dataset is as low as 2%.

Model	Fraction of males (in %)			
Input dataset	2.00	5.00	10.00	20.00
Vanilla GAN	5.23	7.42	12.16	21.29
Robust GAN	4.84	7.80	10.12	21.51

D Biases And Mode Drop

The model of outliers we assume in our paper is that of large noise (Section 3). Hence, our model drops samples that are far from the true data distribution in the Wasserstein sense. It is important

that these dropped samples do not correspond to rare modes in the dataset, or have a mechanism to identify such mode dropping when it happens. In Table. 1, we observe no drop in FID scores on clean CIFAR-10 dataset, which suggests that no mode drop has occurred. To further understand if biases in the dataset are exacerbated, we train our robust Wasserstein GAN model on CelebA dataset with varying male:female ratio. We then measure the male:female ratio of the generated distribution obtained from the trained GAN (using an attribute classifier). Table 6 shows the results. We observe that even when fraction of males in the input dataset are as low as 2%, images of males are generated in robust GAN model. This indicates that rare modes are not dropped. Instead, our robust GAN model drops samples having large noise.

Identifying mode drop: In some cases, as pointed by the reviewer, rare modes can potentially be dropped. In this case, we can use the weights estimated by our weight network $\mathbf{W}(x)$ to visualize which modes are dropped (Fig 3 and 4 of the main paper). Samples with low weights are the ones that are dropped. We can use these weights in a boosting framework to train a mixture model to generate balanced datasets. This is a topic of future research.

E Properties of Robust OT

For a measure to be a distance metric, it has to satisfy four properties of non-negativity, identity, symmetry and triangle inequality.

Non-negativity Robust Wasserstein measure $\mathcal{W}_{\rho_1, \rho_2}^{rob}(\mathbb{P}_X, \mathbb{P}_Y)$ is non-negative. By definition,

$$\mathcal{W}_{\rho_1, \rho_2}^{rob}(\mathbb{P}_X, \mathbb{P}_Y) := \min_{\mathbb{P}_{\tilde{X}}, \mathbb{P}_{\tilde{Y}} \in Prob(\mathcal{X})} \min_{\pi \in \Pi(\mathbb{P}_{\tilde{X}}, \mathbb{P}_{\tilde{Y}})} \int \int c(x, y) \pi(x, y) dx dy$$

s.t. $\mathcal{D}_f(\mathbb{P}_{\tilde{X}} || \mathbb{P}_X) \leq \rho_1, \mathcal{D}_f(\mathbb{P}_{\tilde{Y}} || \mathbb{P}_Y) \leq \rho_2.$

Since the cost function $c(\cdot)$ and the transportation map $\pi(\cdot)$ are non-negative, the robust OT measure is non-negative.

Identity: Robust Wasserstein measure satisfies identity. In other words, $\mathcal{W}_{\rho_1, \rho_2}^{rob}(\mathbb{P}_X, \mathbb{P}_X) = 0$. To prove this, consider the following solution: $\pi(x, y) = 1$ if $x = y$, and $\pi(x, y) = 0$ otherwise, $\mathbb{P}_{\tilde{X}} = \mathbb{P}_X$ and $\mathbb{P}_{\tilde{Y}} = \mathbb{P}_Y$. Clearly, this is a feasible solution. Also, under this solution, the OT cost is 0 as $c(x, x) = 0$. Since, robust OT is non-negative, this is the optimal solution.

Symmetry: In general, robust Wasserstein is not symmetric $\mathcal{W}_{\rho_1, \rho_2}^{rob}(\mathbb{P}_X, \mathbb{P}_Y) = 0 \neq \mathcal{W}_{\rho_1, \rho_2}^{rob}(\mathbb{P}_Y, \mathbb{P}_X) = 0$. This is because when $\rho_1 \neq \rho_2$, different f -divergence constraints are imposed on the two marginals leading to different solutions. However, $\mathcal{W}_{\rho, \rho}^{rob}(\mathbb{P}_X, \mathbb{P}_Y)$ is symmetric. This is because $\int \int c(x, y) \pi(x, y) dx dy = \int \int c(y, x) \pi(y, x) dy dx$, and constraints on two marginals are the same for both optimization problems $\mathcal{W}_{\rho, \rho}^{rob}(\mathbb{P}_X, \mathbb{P}_Y)$ and $\mathcal{W}_{\rho, \rho}^{rob}(\mathbb{P}_Y, \mathbb{P}_X)$.

Triangle inequality: $\mathcal{W}_{\rho_1, \rho_2}^{rob}(\mathbb{P}_X, \mathbb{P}_Y)$ does not satisfy triangle inequality.

F Experiments

F.1 Generative modeling

The formulation of robust Wasserstein GAN is discussed in Section 5 of the main paper. The idea is to modulate the discriminator loss using a weight network $\mathbf{W}(\cdot)$. The output of the $\mathbf{W}(\cdot)$ has a ReLU transform to make it non-negative, and for each batch, the weights are normalized to satisfy $\mathbb{E}_{\mathbf{x} \in \mathbb{P}_X}[\mathbf{W}(\mathbf{x})] = 1$. Then, the objective of robust Wasserstein GAN can be written as

Robust Wasserstein GAN:

$$\min_{\mathbf{W}, \mathbf{G}} \max_{\mathbf{D} \in Lip-1} \mathbb{E}_{\mathbf{x} \sim \mathbb{P}_X}[\mathbf{W}(\mathbf{x})\mathbf{D}(\mathbf{x})] - \mathbb{E}_{\mathbf{z}}[\mathbf{D}(\mathbf{G}(\mathbf{z}))] + \lambda \max(\mathbb{E}_{\mathbf{x} \sim \mathbb{P}_X}[(\mathbf{W}(\mathbf{x}) - 1)^2] - 2\rho, 0)$$

(21)

We can similarly extend the robust GAN formulations to other GAN variants such as spectral normalization GAN or non-saturating GAN as follows.

Robust Non-saturating GAN:

$$\min_{\mathbf{W}, \mathbf{G}} \max_{\mathbf{D}} \mathbb{E}_{\mathbf{x} \sim \mathbb{P}_X} [\mathbf{W}(\mathbf{x}) \log(\mathbf{D}(\mathbf{x}))] + \mathbb{E}_{\mathbf{z}} [\log(1 - \mathbf{D}(\mathbf{G}(\mathbf{z})))] + \lambda \max (\mathbb{E}_{\mathbf{x} \sim \mathbb{P}_X} [(\mathbf{W}(\mathbf{x}) - 1)^2] - 2\rho, 0) \quad (22)$$

Robust Spectral Normalization GAN:

$$\min_{\mathbf{W}, \mathbf{G}} \max_{\mathbf{D}} \mathbb{E}_{\mathbf{x} \sim \mathbb{P}_X} [\mathbf{W}(\mathbf{x}) \max(1 - \mathbf{D}(\mathbf{x}), 0)] + \mathbb{E}_{\mathbf{z}} [\max(1 + \mathbf{D}(\mathbf{G}(\mathbf{z})), 0)] + \lambda \max (\mathbb{E}_{\mathbf{x} \sim \mathbb{P}_X} [(\mathbf{W}(\mathbf{x}) - 1)^2] - 2\rho, 0) \quad (23)$$

Algorithm 1 Robust Wasserstein GAN training algorithm

Require: N_{iter} : Number of training iterations, N_{critic} : Number of critic iterations, N_{batch} : Batch size, N_{weight} : Number of weight update iterations

- 1: **for** t in $1 : N_{iter}$ **do**
- 2: Sample a batch of real samples $\{\mathbf{x}_i\}_{i=1}^{N_{batch}} \sim \mathcal{D}$
- 3: Sample a batch of noise vectors $\{\mathbf{z}_i\}_{i=1}^{N_{batch}} \sim \mathcal{D}$
- 4: Normalize weight vectors as $\mathbf{W}(\mathbf{x}_i) \leftarrow \mathbf{W}(\mathbf{x}_i) / \sum_{i=1}^{N_{batch}} \mathbf{W}(\mathbf{x}_i)$
- 5: Obtain GAN loss as

$$\mathcal{L}_{GAN} = \frac{1}{N_{batch}} \sum_i \mathbf{W}(\mathbf{x}_i) \mathbf{D}(\mathbf{x}_i) - \frac{1}{N_{batch}} \sum_i \mathbf{D}(\mathbf{G}(\mathbf{z}_i)) + \lambda \max \left(\frac{1}{N_{batch}} \sum_i [(\mathbf{W}(\mathbf{x}_i) - 1)^2] - 2\rho, 0 \right) + \lambda_{GP} \frac{1}{N_{batch}} \sum_i (\|\mathbf{D}(\hat{\mathbf{x}}_i)\| - 1)^2$$

- 6: Update discriminator as $\mathbf{D} \leftarrow \mathbf{D} + \eta_D \nabla_{\mathbf{D}} \mathcal{L}_{GAN}$
 - 7: **if** $t \% N_{weight} == 0$ **then**
 - 8: Update weight network as $\mathbf{W} \leftarrow \mathbf{W} - \eta_w \nabla_{\mathbf{W}} \mathcal{L}_{GAN}$
 - 9: **end if**
 - 10: **if** $t \% N_{critic} == 0$ **then**
 - 11: Update generator as $\mathbf{G} \leftarrow \mathbf{G} - \eta_g \nabla_{\mathbf{G}} \mathcal{L}_{GAN}$
 - 12: **end if**
 - 13: **end for**
-

In what follows, we provide more details on the experimental settings used in main paper.

F.1.1 Dataset with outliers

In Section 5.1.1 of the main paper, we show experiments on CIFAR-10 dataset artificially corrupted with MNIST and uniform noise outliers. Each experiment is conducted with a different outlier fraction γ . For a given γ , the outlier-corrupted dataset is constructed so that outliers occupy γ fraction of samples. In all experiments, the total size of the dataset (including outliers) was maintained as 50000. All models were trained using robust Wasserstein loss given in Eq. (21). Experiments were performed on two architectures - DCGAN and Resnet.

For quantitative evaluation, FID scores with respect to clean CIFAR-10 dataset are reported. That is, let m_c and C_c denote the mean and covariance matrices of Inception network features obtained from clean CIFAR-10 dataset (CIFAR-10 without outliers), and m and C denote the mean and covariance of Inception network features obtained from generated samples. Then, the FID score is computed as

$$FID = \|m - m_c\|_2^2 + Tr \left(C + C_c - 2(CC_c)^{1/2} \right).$$

To compute the FID score, the mean and covariance matrices were computed over 50000 samples.

On sketch domain on DomainNet dataset, robust spectral normalization GAN (Eq. (23)) was trained. Resnet architectures were used for both discriminator and generator.

Table 7: Architectures and hyper-parameters: Resnet model

Generator	Discriminator
$z \in \mathbb{R}^{128} \sim \mathcal{N}(0, 1)$	Input $\mathbf{x} \in \mathbb{R}^{32 \times 32 \times 3}$
Dense, $4 \times 4 \times 128$	ResBlock down 128
ResBlock up 128	ResBlock down 128
ResBlock up 128	ResBlock 128
ResBlock up 128	ResBlock 128
BN, ReLU, Conv 3×3	ReLU, Global sum pooling
Tanh	Dense $\rightarrow 1$
Hyperparameters	
Generator learning rate	0.0002
Discriminator learning rate	0.0002
Weight net learning rate	0.0002
Generator optimizer	Adam, Betas (0.0, 0.999)
Discriminator optimizer	Adam, Betas (0.0, 0.999)
Weight net optimizer	Adam, Betas (0.0, 0.999)
Number of critic iterations	5
Weight update iterations	5
Gradient penalty	10
Batch size	128

Table 8: Architectures and hyper-parameters: DCGAN model

Generator	Discriminator
$z \in \mathbb{R}^{128} \sim \mathcal{N}(0, 1)$	Input $\mathbf{x} \in \mathbb{R}^{32 \times 32 \times 3}$
Dense, $4 \times 4 \times 512 + \text{BN} + \text{ReLU}$	Conv 3×3 , str 1, (64) + LReLU
ConvTranspose 4×4 , str 2, (256) + BN + ReLU	Conv 4×4 , str 2, (128) + BN + LReLU
ConvTranspose 4×4 , str 2, (128) + BN + ReLU	Conv 4×4 , str 2, (256) + BN + LReLU
ConvTranspose 4×4 , str 2, (64) + BN + ReLU	Conv 4×4 , str 2, (512) + BN + LReLU
Conv 3×3 , str 1, (3) + TanH	Conv 4×4 , str 1, (1)
Hyperparameters	
Generator learning rate	0.0001
Discriminator learning rate	0.0001
Weight net learning rate	0.0001
Generator optimizer	Adam, Betas (0.5, 0.9)
Discriminator optimizer	Adam, Betas (0.5, 0.9)
Weight net optimizer	Adam, Betas (0.5, 0.9)
Number of critic iterations	5
Weight update iterations	5
Gradient penalty	10
Batch size	128

Table 9: Architectures of weight network

Weight network
Input $\mathbf{x} \in \mathbb{R}^{32 \times 32 \times 3}$
Conv 3×3 , str 1, (64) + ReLU + Maxpool(2×2)
Conv 3×3 , str 1, (128) + ReLU + Maxpool(2×2)
Conv 3×3 , str 1, (256) + ReLU + Maxpool(2×2)
Conv 4×4 , str 1, (1)

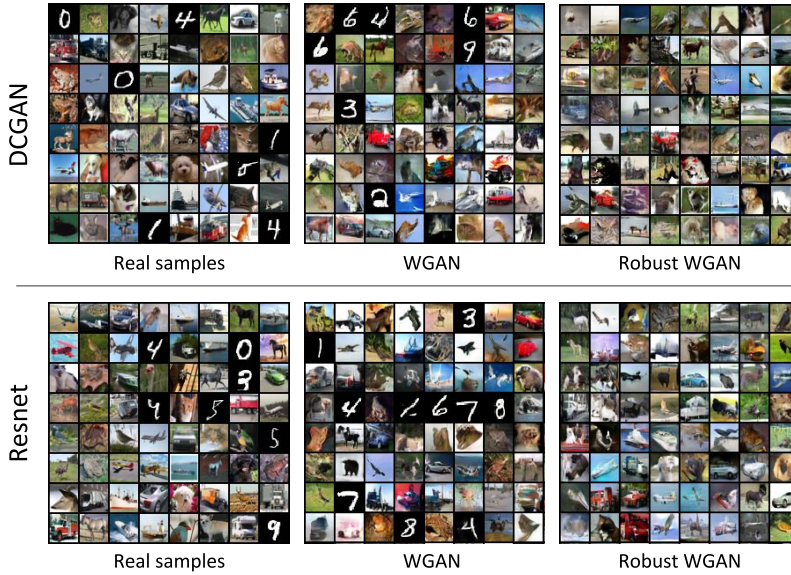


Figure 8: Visualizing samples generated on CIFAR-10 dataset corrupted with MNIST outliers.

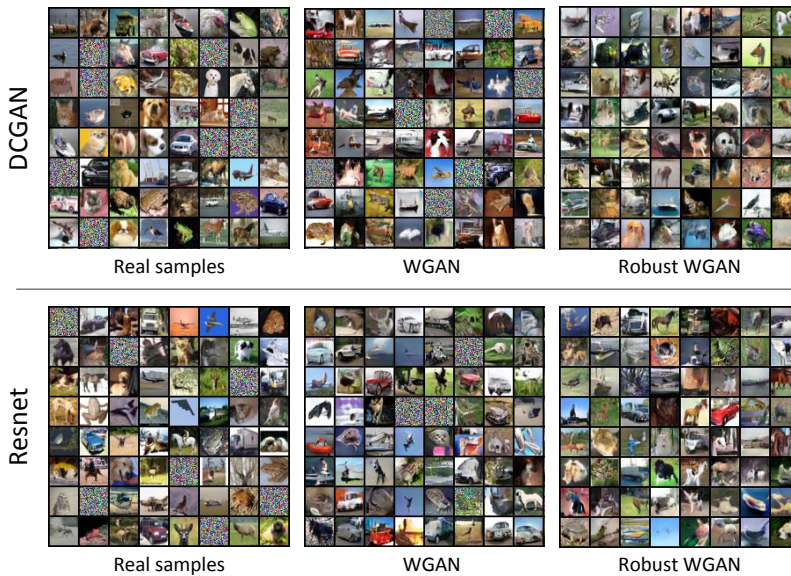


Figure 9: Visualizing samples generated on CIFAR-10 dataset corrupted with uniform noise outliers.

F.1.2 Clean datasets

In Section 5.1.2 of the main paper, robust Wasserstein GANs were trained on clean datasets (datasets with no outlier noise). Experiments were performed on CIFAR-10 and CIFAR-100 datasets. On CIFAR-10, unconditional model was trained, whereas on CIFAR-100, conditional GAN using conditional batch normalization (similar to [18]) was trained.

F.1.3 Architectures and Hyper-parameters

Models and hyperparameters used for DCGAN and Resnet models are provided in Tables 7 and 8. For both models, the architecture used for the weight network is provided in Table 9.

F.2 Domain Adaptation

In all domain adaptation experiments, we update the weight vectors using discrete optimization version discussed in Section 4.3.1 of the main paper. For all models, an entropy regularization on target logits is used. A complete algorithm is provided in Alg. 2. We evaluate our approach on VISDA-17 dataset using Resnet-18, 50 and 101 architectures as discussed in Section 5.2 of the main paper.

Algorithm 2 Domain adaptation training algorithm

Require: N_{iter} : Number of training iterations, N_{critic} : Number of critic iterations, N_{batch} : Batch size, N_{weight} : Number of weight update iterations

- 1: Initialize weight bank $\mathbf{w}_b = [w_1, w_2, \dots, w_{N_t}]$, where each w_i corresponds to weight of target \mathbf{x}_i^t
- 2: **for** t in $1 : N_{iter}$ **do**
- 3: Sample a batch of labeled source images $\{\mathbf{x}_i^s, y_i^s\}_{i=1}^{N_{batch}} \sim \mathcal{D}_s$ and unlabeled target images $\{\mathbf{x}_i^t\}_{i=1}^{N_{batch}} \sim \mathcal{D}_t$
- 4: Obtain the weight vectors w_i^t corresponding to the target samples \mathbf{x}_i^t from the weight bank \mathbf{w}_b
- 5: Obtain discriminator loss as

$$\mathcal{L}_{disc} = \frac{1}{N_{batch}} \sum_i L_{BCE}(\mathbf{D}(\mathbf{F}(\mathbf{x}_i^s)), 0) + \frac{1}{N_{batch}} \sum_i w_i^t L_{BCE}(\mathbf{D}(\mathbf{F}(\mathbf{x}_i^t)), 1)$$

- 6: Obtain source label prediction loss as

$$\mathcal{L}_{cls} = \frac{1}{N_{batch}} \sum_i L_{CE}(\mathbf{C}(\mathbf{F}(\mathbf{x}_i^s)), y_i^s)$$

- 7: Update discriminator $\mathbf{D} \leftarrow \mathbf{D} - \eta_d \nabla_{\mathbf{D}} \mathcal{L}_{disc}$
 - 8: Update feature network and classifier $\mathbf{F} \leftarrow \mathbf{F} - \eta_f \nabla_{\mathbf{F}} \mathcal{L}_{cls}$, $\mathbf{C} \leftarrow \mathbf{C} - \eta_c \nabla_{\mathbf{C}} \mathcal{L}_{cls}$
 - 9: **if** $t \% N_{weight} == 0$ **then**
 - 10: Update weight bank \mathbf{w}_b using Algorithm 3
 - 11: **end if**
 - 12: **if** $t \% N_{critic} == 0$ **then**
 - 13: Update feature network as $\mathbf{F} \leftarrow \mathbf{F} + \eta_f \nabla_{\mathbf{F}} \mathcal{L}_{disc}$
 - 14: **end if**
 - 15: **end for**
-

Algorithm 3 Algorithm for updating weights

- 1: Form the discriminator vector $\mathbf{d} = [\mathbf{D}(\mathbf{x}_1^t), \mathbf{D}(\mathbf{x}_2^t), \dots, \mathbf{D}(\mathbf{x}_{N_t}^t)]$
- 2: Obtain \mathbf{w}_b as the solution of the following second-order cone program

$$\begin{aligned} & \min_{\mathbf{w}} (\mathbf{w})^t \mathbf{d} \\ & \text{s.t. } \|\mathbf{w} - \mathbf{1}\|_2 \leq \sqrt{2\rho_1 N_t} \\ & \mathbf{w} \geq 0, (\mathbf{w})^t \mathbf{1} = N_t \end{aligned}$$

- 3: Return \mathbf{w}_b
-

Baselines: Two standard baselines for the domain adaptation problem include source only and Adversarial alignment. In the source only model, the feature network \mathbf{F} and the classifier \mathbf{C} are trained only on the labeled source dataset. In the adversarial alignment, domain discrepancy between source and target feature distributions is minimized in addition to the source classification loss. This is essentially an unweighted version of our adaptation objective.

Architectures: In our experiments, the feature network \mathbf{F} is implemented using Resnet architectures (Resnet-18, 50 and 101). Following the usual transfer learning paradigm, the last linear layer is removed in the Resnet network. The feature network is initialized with weights pretrained on Imagenet. The classifier network \mathbf{C} is a linear layer mapping the features to probability vector

Table 10: Hyper-parameters for domain adaptation experiments

Hyperparameters	
F network learning rate	0.0005
C network learning rate	0.0005
D network learning rate	0.0001
F network optimizer	SGD with Inv LR scheduler
C network learning rate	SGD with Inv LR scheduler
D network learning rate	Adam betas (0.9, 0.999)
Number of critic iterations	5
Batch size	28
Entropy weight	0.25
Weight update iterations	500
Outlier fraction ρ	0.2

with dimension equal to the number of classes. The classifier network is trained from scratch. The discriminator is realized as a 3-layer MLP with ReLU non-linearities and hidden layer dimension 256. Spectral normalization is used on the discriminator network. The hyper-parameters used in all experiments are described in Table 10.

Weight visualization: We visualize the weights learnt by our domain adaptation module by plotting the histogram of weights in Figure 11. Additionally, target samples sorted by weights are shown in Figure 10.

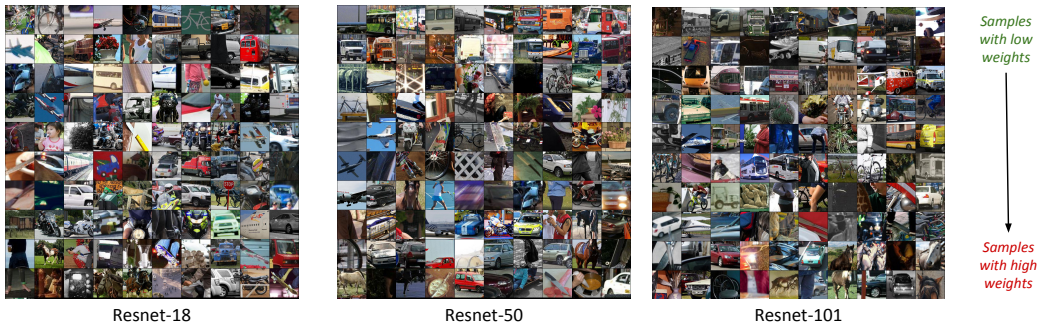


Figure 10: Visualizing target domain samples sorted by learnt weights

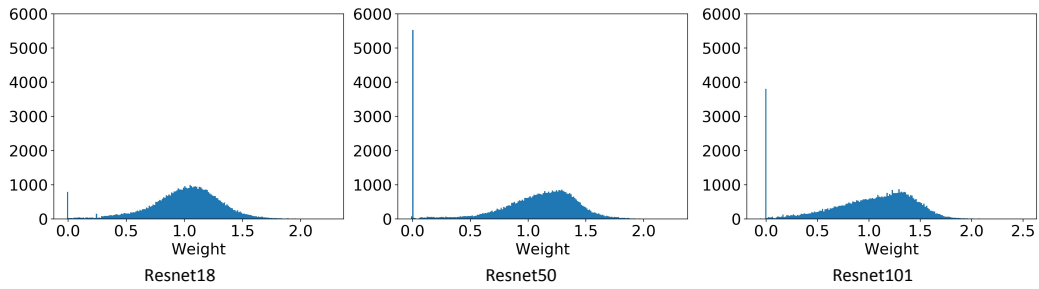


Figure 11: Visualizing histograms of weights learnt in robust domain alignment